J|A|C|S ARTICLES

Published on Web 08/31/2010

Phase Separation and Suppression of the Structural and Magnetic Transitions in Superconducting Doped Iron Tellurides, $Fe_{1+x}Te_{1-y}S_y$

Pawel Zajdel,[†] Ping-Yen Hsieh,[†,‡] Efrain E. Rodriguez,[†] Nicholas P. Butch,[⊥] Jeff D. Magill,[⊥] Johnpierre Paglione,[⊥] Peter Zavalij,[§] Matthew R. Suchomel,[||] and Mark A. Green[†,‡,*]

NIST Center for Neutron Research, NIST, 100 Bureau Drive, Gaithersburg, 20878 Maryland, Departments of Materials Science and Engineering, Center for Nanophysics and Advance Materials and Chemistry, University of Maryland, College Park, Maryland 20742, and Advanced Photon Source, Argonne National Laboratory, Argonne, Illinois 60439

Received June 16, 2010; E-mail: mark.green@nist.gov

Abstract: Single crystal and powder samples of the series of iron chalcogenide superconductors with nominal composition, $Fe_{1.15}Te_{1-y}S_y$, are found to form for $0 \le y \le 0.15$. They crystallize in the tetragonal anti-PbO structure, which is composed of layers of edge-shared Fe(Te, S)$_4$ tetrahedra. For $y = 0$, $Fe_{1+x}Te$ ($x \approx 0.12(1)$) is nonsuperconducting and undergoes a tetragonal ($P4/nmm$) to monoclinic ($P2_1/m$) structural transition at ~65 K, associated with the onset of commensurate antiferromagnetic order at $\mathbf{q} = (0.5\ 0\ 0.5)$. We show that on sulfur substitution, $Fe_{1+x}Te_{1-y}S_y$ becomes orthorhombic ($Pmmn$) at low temperature for $0 \le y \le 0.015$, where the greatly suppressed magnetic scattering is now incommensurate at $\mathbf{q} = (0.5\text{-}\delta\ 0\ 0.5)$ and possesses short ranged magnetic correlations that are well fitted with a two-dimensional Warren peak shape. At much higher concentrations of S ($y \ge 0.075$), there is suppression of both the structural and magnetic transitions and a superconducting transition at 9 K is observed. Between these two composition regimes, there exists a region of phase separation ($0.025 \le y \le 0.05$), where the low temperature neutron diffraction data is best refined with a model containing both the tetragonal and orthorhombic phases. The increase in the amount of sulfur is found to be associated with a reduction in interstitial iron, x. Microprobe analysis of a single crystal of composition $Fe_{1.123(5)}Te_{0.948(4)}S_{0.052(4)}$ confirms the presence of compositional variation within the crystals, rationalizing the observed phase separation.

Introduction

The discovery of superconductivity in $LaO_{1-x}F_xFeAs$ at 26 K[1] marked the onset of establishing a new category of high temperature superconductors based on iron. This ZrCuSiAs-type compound contains alternating layers of PbO-type LaO and the electronically active anti-PbO-type FeAs blocks. It was shown that variation of lanthanide ion greatly affects the superconducting transition temperatures from $CeO_{1-x}F_xFeAs$ (T_C = 41 K),[2] $NdO_{1-x}F_xFeAs$ (T_C = 51 K),[3] $PrO_{1-x}F_xFeAs$ (T_C = 52 K),[4] to $SmO_{1-x}F_xFeAs$ (T_C = 55 K).[5] Superconductivity in alternative structures was later found in the related $ThCr_2Si_2$-type system, AFe_2As_2 (A = Ba, Sr, Ca)[6,7] and anti-PbFCl structure, AFeAs (A = Na or Li).[8−10] The same fundamental structural building block in these systems, the FeAs layers, crystallizes without the need of cations in the form of the tetragonal anti-PbO structure, shown in Figure 1, now with doubly charged anions required to maintain the Fe^{2+} oxidation state, such as in the series Fe(Te, Se, S). In this family, FeTe is superconducting with either Se[11] and S[12] inclusion, whereas stoichiometric FeSe[13,14] is superconducting at temperatures as high as 36.7 K under pressure.[15,16] More recently, it has been

[†] NIST.
[‡] Materials Science and Engineering, University of Maryland.
[⊥] Center for Nanophysics and Advance Materials, University of Maryland.
[§] Chemistry, University of Maryland.
[||] APS.

(1) Kamihara, Y.; Watanabe, T.; Hirano, M.; Hosono, H. *J. Am. Chem. Soc.* **2008**, *130*, 3296.
(2) Chen, G. F.; Li, Z.; Wu, D.; Li, G.; Hu, W. Z.; Dong, J.; Zheng, P.; Luo, J. L.; Wang, N. L. *Phys. Rev. Lett.* **2008**, *100*, 247002.
(3) Ren, Z. A.; Yang, J.; Lu, W.; Yi, W.; Shen, X. L.; Li, Z. C.; Che, G. C.; Dong, X. L.; Sun, L. L.; Zhou, F.; Zhao, Z. X. *EPL* **2008**, *82*, 57002.
(4) Ren, Z. A.; Yang, J.; Lu, W.; Yi, W.; Che, G. C.; Dong, X. L.; Sun, L. L.; Zhao, Z. X. *Mater. Res. Innovation* **2008**, *12*, 105.
(5) Ren, Z. A.; Lu, W.; Yang, J.; Yi, W.; Shen, X. L.; Li, Z. C.; Che, G. C.; Dong, X. L.; Sun, L. L.; Zhou, F.; Zhao, Z. X. *Chin. Phys. Lett.* **2008**, *25*, 2215.
(6) Rotter, M.; Tegel, M.; Johrendt, D. *Phys. Rev. Lett.* **2008**, *101*, 107006.
(7) Chen, G. F.; Li, Z.; Li, G.; Hu, W. Z.; Dong, J.; Zhou, J.; Zhang, X. D.; Zheng, P.; Wang, N. L.; Luo, J. L. *Chin. Phys. Lett.* **2008**, *25*, 3403.
(8) Pitcher, M. J.; Parker, D. R.; Adamson, P.; Herkelrath, S. J. C.; Boothroyd, A. T.; Ibberson, R. M.; Brunelli, M.; Clarke, S. J. *Chem. Commun.* **2008**, 5918.
(9) Wang, X. C.; Liu, Q. Q.; Lv, Y. X.; Gao, W. B.; Yang, L. X.; Yu, R. C.; Li, F. Y.; Jin, C. Q. *Solid State Commun.* **2008**, *148*, 538.
(10) Parker, D.; Vavilov, M.; Chubukov, A.; Mazin, I. *Phys. Rev. B* **2009**, *80*, 100508.
(11) Yeh, K. W.; Huang, T. W.; Huang, Y. L.; Chen, T. K.; Hsu, F. C.; Wu, P. M.; Lee, Y. C.; Chu, Y. Y.; Chen, C. L.; Luo, J. Y.; Yan, D. C.; Wu, M. K. *EPL* **2008**, *84*, 37002.
(12) Mizuguchi, Y.; Tomioka, F.; Tsuda, S.; Yamaguchi, T.; Takano, Y. *Appl. Phys. Lett.* **2009**, *94*, 012503.

 10.1021/ja105279p

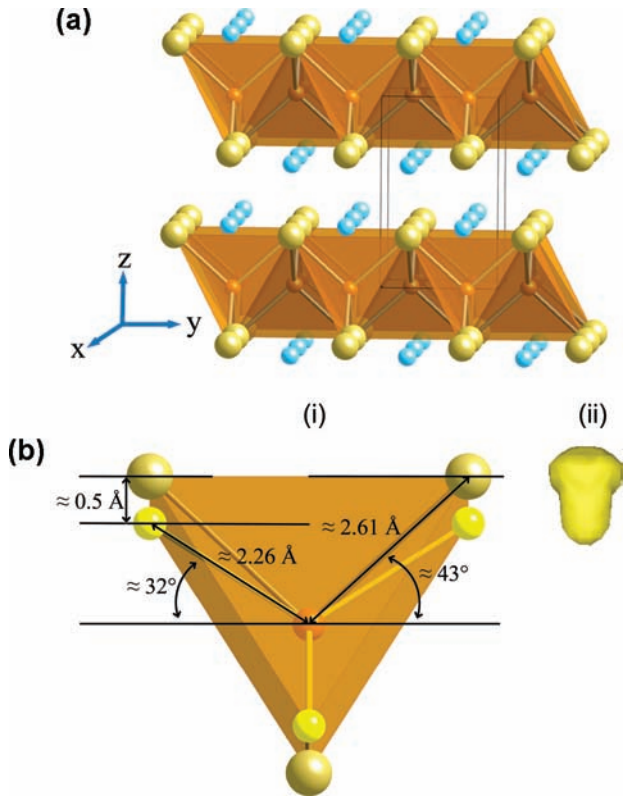

Figure 1. (a) The anti-PbO-type structure of $Fe_{1-x}Te$, composed of layers of tetragonal Fe(1) (orange) − Te (yellow) units lying in the *xy* plane, separated along the *z* axis by partially occupied Fe(2) interstitial sites. Sulfur doping occurs on the Tellurium sites. (b) (i) The structure of $Fe_{1.123(5)}Te_{0.948(4)}S_{0.052(4)}$ as determined by single crystal X-ray diffraction, showing the distinct positions for Te and S, that was confirmed with (ii) reconstruction of the nuclear scattering density using the maximum entropy analysis of the powder neutron diffraction data of $Fe_{1+x}Te_{0.9}S_{0.1}$.

suggested that $Fe_{1+x}Te$ can support superconductivity at $T_C \approx$ 13 K when grown in thin film form.[17]

The structural simplicity of Fe(Te, Se, S) systems, along with their propensity to form high quality single crystals, lends this family of superconductors to extensive research on their structure, magnetism, and sample homogeneity. One central issue in iron-based superconductivity, which is controlled by both composition and/or pressure, is the competition at low temperature between high (tetragonal) and low (orthorhombic or monoclinic) crystal symmetry; the former is associated with superconductivity, whereas the latter is concomitant with the appearance of a localized moment and no superconductivity.[18−23]

The structural phase diagram of the Fe(Te, Se, S) series is one of the many important differences that distinguishes it from other families of iron-based superconductors. For example, FeSe is superconducting at $T_C \approx 8.5$ K, is orthorhombic rather than tetragonal at low temperature, yet displays no long ranged magnetic order.[13,14,24] Pressure has a dramatic effect on the superconducting transition temperature,[15] increasing it to 36.7 K at 8.9 GPa, as a result of the markedly reduced interlayer separation, before transforming to a nonsuperconducting NiAs-type structure at higher pressures.[16] $Fe_{1+x}Te$ possesses additional structural complexity as a result of the presence of secondary interstitial Fe ions between the anti-PbO-like blocks. This has important consequences on both its structure and magnetism; $Fe_{1+x}Te$ undergoes a low temperature distortion from tetragonal to monoclinic at $x \leq 0.12$, which is associated with the onset of commensurate antiferromagnetic order at $\mathbf{q} = (1/2\ 0\ 1/2)$, whereas an orthorhombic symmetry is present at $x > 0.12$, which has incommensurate antiferromagnetic order at $\mathbf{q} = (1/2\text{-}\delta\ 0\ 1/2)$.[23] For all compositions the localized moment at $\sim 2\,\mu_B$[23] in the parent compositions is significantly higher than that found in other structural families and with a different propagation vector that is rotated by 45° compared with other structural families, giving a unique double stripe feature.[19−22,25] A comprehensive study of the $Fe_{1+y}Te_{1-x}S_x$ demonstrated the importance of stoichiometry in these compounds and correlation between magnetism and superconductivity that warrants a detailed structural study.[26]

Here we show that on S doping the commensurate antiferromagnetic and monoclinic structure of $Fe_{1+x}Te$ first becomes orthorhombic, with incommensurate short ranged two-dimensional antiferromagnetic correlations, before complete suppression of both the magnetic and structural transitions leads to a tetragonal superconductor at $T_C \sim 9$ K. Compositional variation within the samples accounts for a phase separated region between the orthorhombic and tetragonal regimes. Increasing the amount of sulfur dopant on the Te sites also reduced the amount of interstitial iron, therefore the observed changes in the magnetism is likely a result of both of these factors. These results further stress the uniqueness of the Fe(Te, Se, S) phase diagram compared with the other iron based superconductors, although the observed superconducting transition temperature and tetrahedral bond variance is consistent with all families of iron-based superconductors.

Experimental Details

Powder samples of $Fe_{1+x}Te_{1-y}S_y$ ($0 < y < 0.15$) were synthesized by direct reaction of Fe, Te, and S in an evacuated sealed quartz

(13) Hsu, F.; Luo, J.; Yeh, K.; Chen, T.; Huang, T.; Wu, P.; Lee, Y.; Huang, Y.; Chu, Y.; Yan, D.; Wu, M. *Proc. Natl. Acad. Sci. U.S.A.* **2008**, *105*, 14262.
(14) McQueen, T. M.; Huang, Q.; Ksenofontov, V.; Felser, C.; Xu, Q.; Zandbergen, H.; Hor, Y. S.; Allred, J.; Williams, A. J.; Qu, D.; Checkelsky, J.; Ong, N. P.; Cava, R. J. *Phys. Rev. B* **2009**, *79*, 014522.
(15) Mizuguchi, Y.; Tomioka, F.; Tsuda, S.; Yamaguchi, T.; Takano, Y. *Appl. Phys. Lett.* **2008**, *93*, 152505.
(16) Medvedev, S.; Mcqueen, T. M.; Troyan, I. A.; Palasyuk, T.; Eremets, M. I.; Cava, R. J.; Naghavi, S.; Casper, F.; Ksenofontov, V.; Wortmann, G.; Felser, C. *Nat. Mater.* **2009**, *8*, 630.
(17) Han, Y.; Li, W. Y.; Cao, L. X.; Wang, X. Y.; Xu, B.; Zhao, B. R.; Guo, Y. Q.; Yang, J. L. *Phys. Rev. Lett.* **2010**, *104*, 017003.
(18) de la Cruz, C.; Huang, Q.; Lynn, J. W.; Li, J. Y.; Ratcliff, W.; Zarestky, J. L.; Mook, H. A.; Chen, G. F.; Luo, J. L.; Wang, N. L.; Dai, P. C. *Nature* **2008**, *453*, 899.
(19) Zhao, J.; Huang, Q.; de la Cruz, C.; Li, S. L.; Lynn, J. W.; Chen, Y.; Green, M. A.; Chen, G. F.; Li, G.; Li, Z.; Luo, J. L.; Wang, N. L.; Dai, P. C. *Nat. Mater.* **2008**, *7*, 953.
(20) Qiu, Y.; Bao, W.; Huang, Q.; Yildirim, T.; Simmons, J. M.; Green, M. A.; Lynn, J. W.; Gasparovic, Y. C.; Li, J.; Wu, T.; Wu, G.; Chen, X. H. *Phys. Rev. Lett.* **2008**, *101*, 257002.
(21) Huang, Q.; Qiu, Y.; Bao, W.; Green, M. A.; Lynn, J. W.; Gasparovic, Y. C.; Wu, T.; Wu, G.; Chen, X. H. *Phys. Rev. Lett.* **2008**, *101*, 257003.
(22) Kreyssig, A.; Green, M. A.; Lee, Y.; Samolyuk, G. D.; Zajdel, P.; Lynn, J. W.; Bud'ko, S. L.; Torikachvili, M. S.; Ni, N.; Nandi, S.; Leao, J. B.; Poulton, S. J.; Argyriou, D. N.; Harmon, B. N.; McQueeney, R. J.; Canfield, P. C.; Goldman, A. I. *Phys. Rev. B* **2008**, *78*, 184517.
(23) Bao, W.; Qiu, Y.; Huang, Q.; Green, M. A.; Zajdel, P.; Fitzsimmons, M. R.; Zhernenkov, M.; Chang, S.; Fang, M.; Qian, B.; Vehstedt, E. K.; Yang, J.; Pham, H. M.; Spinu, L.; Mao, Z. Q. *Phys. Rev. Lett.* **2009**, *102*, 247001.
(24) Margadonna, S.; Takabayashi, Y.; McDonald, M. T.; Kasperkiewicz, K.; Mizuguchi, Y.; Takano, Y.; Fitch, A. N.; Suard, E.; Prassides, K. *Chem. Commun.* **2008**, 5607.
(25) Qiu, Y.; Kofu, M.; Bao, W.; Lee, S.; Huang, Q.; Yildirim, T.; Copley, J.; Lynn, J.; Wu, T.; Wu, G.; Chen, X. *Phys. Rev. B* **2008**, *78*, 052508.
(26) Hu, R.; Bozin, E. S.; Warren, J. B.; Petrovic, C. *Phys. Rev. B* **2009**, *80*, 214514.

tubes. All materials were heated for 2 days at 450 °C for 6 h to initially react all of the Te, followed by heating at 775 °C for 2 days to form the tetragonal anti-PbO phase. Starting compositions had a fixed nominal Fe content of $x = 0.15$ excess, which proved to be optimal in the formation of single phase material free from $FeTe_2$ and the hexagonal FeTe impurities. Iron loss occurs during the thermal treatment and final iron compositions were determined by a combination of single crystal X-ray diffraction, powder neutron diffraction and microprobe analysis. Samples with higher sulfur content ($y > 0.15$) showed inclusion of FeS as an impurity and lattice parameters comparable to the $x = 0.15$ composition, demonstrating the end of the solid solution under these synthesis conditions, as shown in Figure S1.

Single crystals for X-ray diffraction were silver-black plates of approximate dimension $0.01 \times 0.2 \times 0.2$ mm^3. Data were collected at 250 (2) K on a three-circle diffractometer system equipped with commercial CCD area detector using a graphite monochromator and a Mo Kα fine-focus sealed tube ($\lambda = 0.71073$ Å). The detector was placed at a distance of 5.2 cm from the crystal. Powder neutron diffraction was performed on the BT1 high resolution diffractometer at the NIST Center for Neutron research. Data were collected using the Ge (311) monochromator at $\lambda = 2.0782$ Å and the Cu (311) monochromator at $\lambda = 1.5401$ Å, with an in-pile collimation of 15′. Rietveld refinement was performed using the GSAS[27] and Fullprof[28] packages. Chemical composition analysis was performed using a commerical electron microprobe in wavelength-dispersive spectrometry (WDS) mode. The electron accelerating voltage was 20 kV providing beam of around 10 μm in diameter. High resolution synchrotron powder diffraction data were collected using beamline 11-BM at the Advance Photon Source, Argonne National Laboratory. The scan step size was 0.001° 2θ at a wavelength of $\lambda = 0.458737$ Å. Electrical resistivity measurements were performed in a commercial cryostat on single crystals using a 4-wire geometry.

Results

Single Crystals of $Fe_{1+x}Te_{1-y}S_y$. Single crystal X-ray diffraction of a crystal with nominal composition $Fe_{1.15}Te_{0.95}S_{0.05}$ was refined at 250 (2) K in the *P4/nmm* tetragonal symmetry, yielding an actual stoichiometry of $Fe_{1.123(5)}Te_{0.948(4)}S_{0.052(4)}$. The structure of the anti-PbO structure is given in Figure 1a. Although within experimental error the Te:S ratio is exactly the starting composition, the amount of interstitial iron is lower than expected, which has been previously reported.[23] One of the most significant features of the sulfur doped iron telluride structure is the significant shifting of the sulfur position from the Te site. Figure 1b shows a detailed layout of the Fe tetrahedron. The majority ion, Te, lies at a position at ~2.61 Å from Fe at the center of the tetrahedron and at an angle of ~43° from the (*a b* 0.5) plane, whereas S is significantly closer to Fe at ~2.26 Å and at only ~32° from Fe plane. These values are entirely consistent with the values obtain for the pure phase of FeS (Mackinawite), which shows a Fe−S bond distance of 2.231 Å,[29] and the pure anti-PbO structure of FeTe that gives an identical bond distance of around 2.6 Å.[30] This type of position splitting results from the very large difference in the ionic radii of the two anions and has previously been observed in Fe(Te, Se).[31] To further elucidate the exact distribution of anions, a reconstruction of the nuclear density using the maximum entropy technique was performed on powder neutron diffraction data obtained at 4 K from a powder sample of similar composition, $Fe_{1+x}Te_{0.9}S_{0.1}$. This technique is well established to offer unbiased information on the scattering density, and nuclear density is insensitive to covalency effects apparent from X-ray scattering from the electron distribution. This data formed a series of experiments that is later discussed in full. Neutron diffraction was used as its nuclear scattering gives a clearer distribution of density. The reconstruction of the nuclear scattering density of the combined (Te, S) site is shown in Figure 1b(ii) and confirms the very distinct positions of the two anions. This shifting of the S sites gives a Te - S separation of around 0.5 Å, and its variation with composition is discussed later.

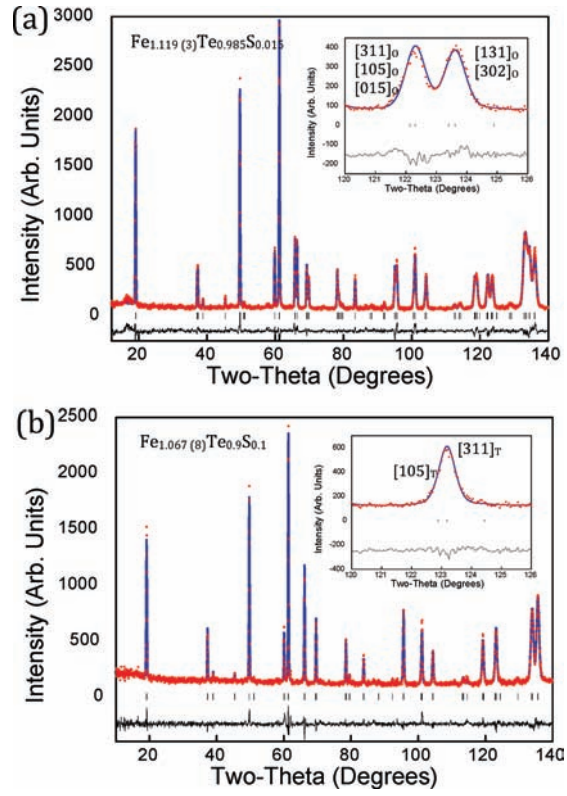

Figure 2. Observed (red circles), calculated (blue line), and difference (black line) of the powder neutron diffraction profile of (a) $Fe_{1.119(3)}Te_{0.985}S_{0.015}$ at 4 K and (b) $Fe_{1.067(8)}Te_{0.9}S_{0.1}$ at 4 K obtain from Rietveld refinement.

Magnetic Structure of $Fe_{1+x}Te_{1-y}S_y$. Low temperature powder neutron diffraction experiments performed at 4 K, an example of which is given in Figure 2, confirmed a dramatic change in the magnetism as a function of sulfur doping. Figure 3a shows the principal magnetic reflection, located to the left of the nuclear (001) reflection at around 19° 2θ, for several compositions of $Fe_{1+y}Te_{1-x}S_x$. For $x = 0$, the commensurate magnetic reflection occurs at propagation vector, $\mathbf{q} = (0.5\ 0\ 0.5)$ and the structure was refined in the monoclinic $P2_1/m$ space group, consistent with previous measurements.[23] The refined composition of $Fe_{1.122(6)}Te$ represents the upper limit of the commensurate monoclinic $Fe_{1+x}Te$ phases, compositions with greater interstitial Fe content are susceptible to incommensurate antiferromagnetic order that is associated with an orthorhombic structure of *Pmmn* symmetry.[23] The inclusion of small amounts of S in $Fe_{1+x}Te_{1-y}S_y$ ($y = 0.0075$, 0.015, and 0.025) shows an immediate alteration of the magnetic ground state; all of these phases are now incommensurate despite the decreased amount of

(27) Larson, A. C.; Von Dreele, R. B.; *Los Alamos National Laboratory Report LAUR 86−748*; Los Alamos National Laboratory: Los Alamos, NM, 1994.
(28) Rodriguez-Carvajal, J. *Phys. B* **1993**, *192*, 55.
(29) Berner, R. A. *Science* **1962**, *137*, 669.
(30) Haraldsen, H.; Groenvol, F.; Vihovde, J. *Tidsskr. Kjemi Bergves.* **1944**, *4*, 96.
(31) Tegel, M.; Lohnert, C.; Johrendt, D. *Solid State Commun.* **2010**, *150*, 383.

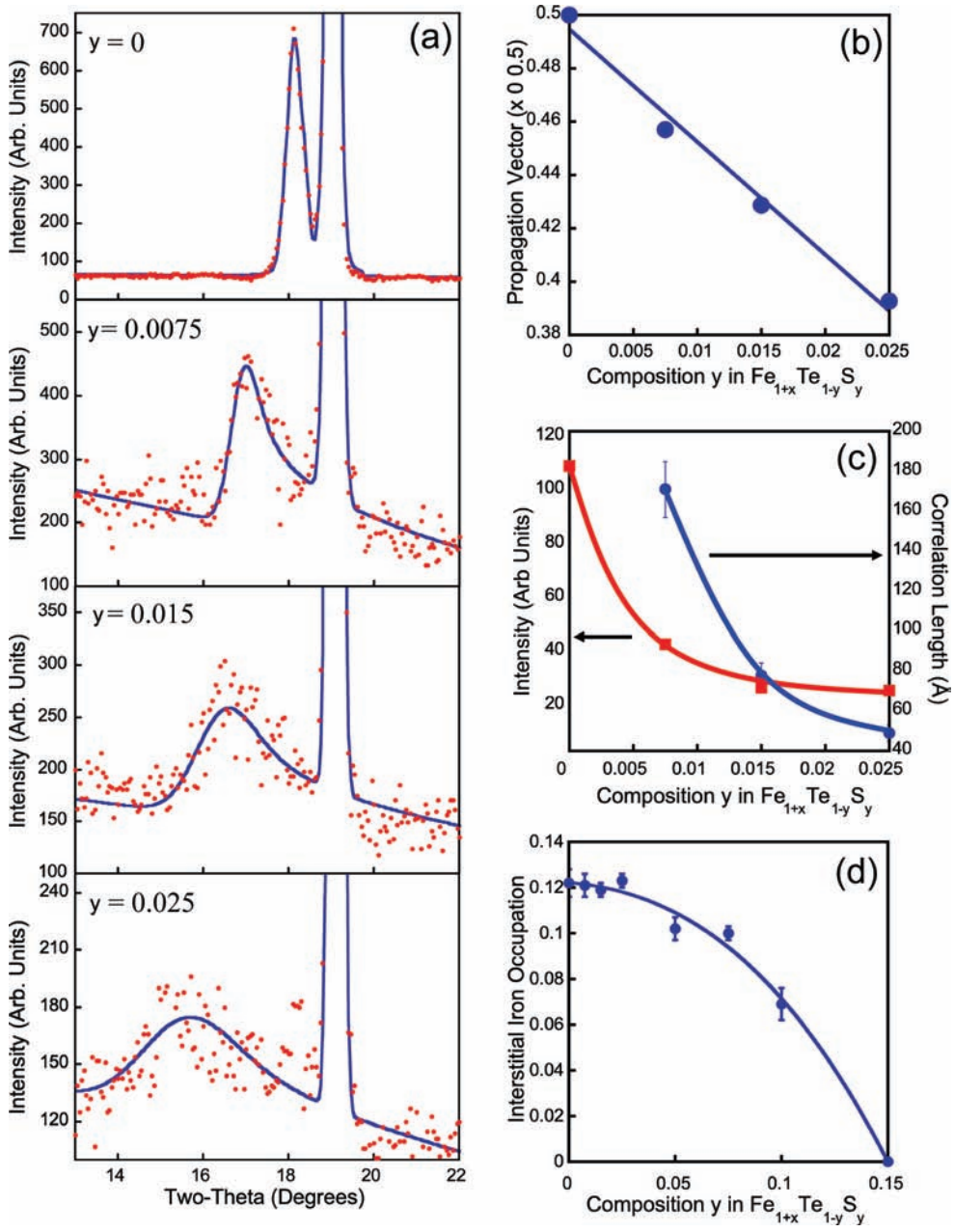

Figure 3. (a) Section of the powder neutron diffraction data for nominal compositions, $Fe_{1.15}Te$, $Fe_{1.15}Te_{0.9925}S_{0.0075}$, $Fe_{1.15}Te_{0.9985}S_{0.015}$, and $Fe_{1.15}Te_{0.9975}S_{0.025}$ (top to bottom), showing a large reduction in ordered moment on S inclusion in the $Fe_{1.15}Te$ lattice leading a transition from a commensurate $\mathbf{q} = (0.5\ 0\ 0.5)$ propagation vector to an incommensurate one. The pattern for $Fe_{1+x}Te$ is from Rietveld refinement analysis, whereas the broad asymmetry magnetic scattering for S doped compounds are fitted to a Warren peak shape, implying the magnetism exhibits short ranged two-dimensional correlation. (b) Variation of the magnetic propagation vector as a function of sulfur doping. (c) Variation of the magnetic intensity and magnetic correlation length as a function of sulfur doping. (d) Variation of interstitial Fe ions as a function of sulfur doping, as determined by Rietveld refinement of powder neutron diffraction data.

interstitial Fe due to the increased S content. The opposite trend has been observed in the $Fe_{1+x}Te$ phases, where decreasing the amount of interstitial Fe tends to stabilize the commensurate antiferromagnetic structure.

Another interesting effect on the magnetic properties with S doping was found by analyzing the peak profile shape of the magnetic reflections. The intensity of the magnetic reflection at $\mathbf{q} = (0.5\text{-}\delta\ 0\ 0.5)$ decreases, while the peak width increases. Such short-range incommensurate magnetic scattering was previously been observed for the $Fe_{1+x}Te_{1-y}Se_y$ system.[23] The asymmetric peak profile shape of this magnetic scattering is indicative of two-dimensional correlations. Therefore these reflections were fitted with a Warren peak shape function[32] that allows for the direct extraction of magnetic correlation length. Figure 3, panels b and c, shows how the magnetic propagation vector, intensity and correlation length varies as a function of S doping. For $y \geq 0.05$ in $Fe_{1+x}Te_{1-y}S_y$, the magnetic scattering was either not present or too broad to measure, indicative of a very rapid suppression of the magnetic scattering as a function sulfur doping (~5%).

Structure and Stoichiometry of $Fe_{1+x}Te_{1-y}S_y$. The apparent difference in the interstitial iron inclusion from the nominal stoichiometry that was observed with single crystal X-ray diffraction was further evaluated as a function of y in

(32) Warren, B. *Phys. Rev.* **1941**, *59*, 693.

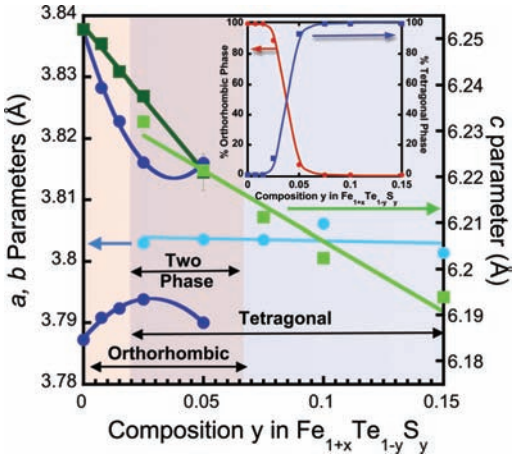

Figure 4. Lattice parameters of the $Fe_{1+x}Te_{1-y}S_y$ series at 4 K, showing the evolution from the orthorhombic *Pmmn* symmetry (*a* dark blue, *c* dark green). Phase separated compositions, where the neutron powder diffraction data was best fitted with a two-phase model, lies between $0.025 \leq x \leq 0.075$, before the appearance of the superconducting tetragonal *P*4/*nmm* phase (*a* light blue, *c* light green). Solubility limit was $x \approx 0.15$ under these synthesis conditions.

$Fe_{1+x}Te_{1-y}S_y$ by Rietveld refinement of the structure with powder neutron diffraction data. Figure 3d shows the observed amount of interstitial iron on the secondary Fe site as a function of S doping. As found for Fe_{1+x}(Te,Se),[33] there is a correlation such that the amount of interstitial iron decreases with increases substitution of Te with the smaller anion.

Structural refinements using the powder neutron diffraction data at 4 K, shows that within the incommensurate magnetic regime of $Fe_{1+x}Te_{1-y}S_y$ ($0.0075 \leq y \leq 0.025$), the crystal structure is orthorhombic with the *Pmmn* space group; the same space group employed in the incommensurate phases of $Fe_{1+x}Te$ with $x > 0.12$. At much higher concentrations of S ($y \geq 0.05$), the best single phase fit occurs in the tetragonal *P*4/*nmm* space group present at high temperature, implying the absence of a low temperature distortion with higher S doping. However the quality of the fits at 4 K for composition of $Fe_{1+x}Te_{1-y}S_y$ between $0.025 \leq y \leq 0.05$ were noticeably worse and gave higher goodness-of-fit factors. Further Rietveld refinements employing a two-phase model that included both an orthorhombic *Pmmn* phase and a tetragonal *P*4/*nmm* phase gave markedly improved fits to the data. A summary of the structural phase diagram showing the lattice parameters as a function of composition for $Fe_{1+x}Te_{1-y}S_y$ at 4 K is given in Figure 4, outlining the transformation from monoclinic, to orthorhombic, to a phase-separated regime before the tetragonal phase is stable over all temperatures. The inset to Figure 4 shows the phase fraction of the tetragonal and orthorhombic structures as a function of sulfur doping. The structural parameters obtained from Rietveld refinements of powder neutron diffraction data at 4 K are given in Table 1. The inclusion of the S makes remarkable little difference to the bond lengths and angles despite the changes in structural symmetry and magnetism. Figure 5a shows the three key iron bond distances, Fe−Fe2, Fe−Te, and Fe−S, as a function of composition. For all compositions the Fe−Te and Fe−S remain flat around 2.6 and 2.21 Å, respectively, as observed in the single crystal study. The Fe−Fe2 does get significantly longer with higher sulfur composition, this reflects a shifting of the interstitial iron further out of the Te plane and closer to the adjacent Fe−(Te,S) layer. The bond angles of Te−Fe−Te are highly distorted from the ideal tetrahedron value of 109.47° at around 117° and 95°, and are largely unaffected by S composition, see Figure 5b. The difference in length between the Te and S sites, or Te−S separation, shown in Figure 5c, is constant at just over 0.5 Å for the tetragonal section of the phase diagram. There is some indication that this separation increases on reducing S content, but the reducing sensitivity with such low concentrations of S limits any definitive conclusions.

To further elucidate the origin of the phase separation a series of high-resolution synchrotron X-ray powder diffraction experiments were performed, as well as a microprobe analysis of a single crystal of nominal composition $Fe_{1.15}Te_{0.95}S_{0.05}$. Figure 6a shows a comparison of the peak width of the (001) reflection of $Fe_{1+x}Te_{1-y}S_y$ ($y = 0.1$, 0.125, and 0.15) compared with a LaB_6 NIST 660a standard at ambient temperature, confirming that there is considerable sample broadening that was not apparent in the neutron powder diffraction data. Such broadening commonly occurs when there is a distribution of compositions on a microscopic level that is averaged in a diffraction experiment. To explore how this distribution manifested itself within a single crystal, microprobe analysis measurements were performed at 39 positions across a single crystal previously determined by single crystal X-ray diffraction to be of composition, $Fe_{1.123(5)}Te_{0.948(4)}S_{0.052(4)}$. An *xy* map of the determined compositions is given in Figure 6b and demonstrates a continuous variation of the amount of S present within the samples from one end of the crystal to the other.

Superconductivity. A series of resistivity measurements was performed to evaluate the superconducting properties of the $Fe_{1+x}Te_{1-y}S_y$ series. A comparison is shown in the supplementary data between $Fe_{1+x}Te_{0.85}S_{0.15}$ and $Fe_{1+x}Te_{0.875}S_{0.125}$, which shows superconductivity at $T_c \approx 9$ K, which is consistent with previous measurements.[26,33]

Discussion

The substitution of Te (ionic radii = 2.21 Å) for the smaller S (ionic radii = 1.84 Å) ion, predictably reduces both lattice parameters and volume. However, the higher S content also has the effect of reducing the amount of interstitial Fe, which further promotes the contracting volume trend, until no interstitial iron is observed for $y = 0.15$. In the study by Hu et al on $Fe_{1+x}Te_{1-y}S_y$, a similar reduction of the interstitial iron was observed.[26] It is interesting to note that the optimal superconductivity in $Fe_{1+x}Te_{1-y}S_y$ at $y \approx 0.15$, arises in the samples without interstitial iron, which has previously been observed for the selenide series, $Fe_{1+x}Te_{1-y}Se_y$.[33] First principal calculations have predicted that the large localized moment observed on this site in $Fe_{1+x}Te$ is likely to have a detrimental effect on the superconductivity.[34,35] However, it is unclear whether the role of the S substitution is to apply chemical pressure on the system by contracting the lattice and thereby promoting superconductivity, or whether it simply suppresses the inclusion of interstitial Fe ions and stabilizes a stoichiometric and superconducting material. A similar question was answered in the $Fe_{1+x}Se$ system, where it was found that superconductivity was destroyed at $x > 0.01$.[14]

(33) Sales, B. C.; Sefat, A. S.; McGuire, M. A.; Jin, R. Y.; Mandrus, D.; Mozharivskyj, Y. *Phys. Rev. B* **2009**, *79*, 094521.
(34) Han, M. J.; Savrasov, S. Y. *Phys. Rev. Lett.* **2009**, *103*, 067001.
(35) Zhang, L. J.; Singh, D. J.; Du, M. H. *Phys. Rev. B* **2009**, *79*, 012506.

Table 1. Structural Parameters from Rietveld Refinement of Powder Neutron Diffraction Data All Collected at 4 K[a]

parameter	$Fe_{1+x}Te_{0.9925}S_{0.0075}$	$Fe_{1+x}Te_{0.985}S_{0.015}$	$Fe_{1+x}Te_{0.975}S_{0.025}$		$Fe_{1+x}Te_{0.95}S_{0.05}$		$Fe_{1+x}Te_{0.925}S_{0.075}$	$Fe_{1+x}Te_{0.9}S_{0.1}$	$Fe_{1+x}Te_{0.985}S_{0.15}$
crystal system	orthorhombic	orthorhombic	orthorhombic	tetragonal	orthorhombic	tetragonal	tetragonal	tetragonal	tetragonal
propagation vector	(0.4570 (3) 0 0.5)	(0.4286 (3) 0 0.5)	(0.3926 (2) 0 0.5)						
symmetry	*Pmmn*	*Pmmn*	*Pmmn*	*P4/nmm*	*Pmmn*	*P4/nmm*	*P4/nmm*	*P4/nmm*	*P4/nmm*
a (Å)	3.8280 (2)	3.8232 (1)	3.8163 (1)	3.8029 (5)	3.8186 (14)	3.80378 (9)	3.8036 (1)	3.80629 (24)	3.80215 (15)
b (Å)	3.7912 (2)	3.7927 (1)	3.7940 (1)		3.7856 (12)				
c (Å)	6.2484 (3)	6.2434 (2)	6.2378 (2)	6.2324 (18)	6.221 (4)	6.22159 (18)	6.2114 (2)	6.2026 (5)	6.19481 (28)
volume ($Å^3$)	90.680 (8)	90.531 (5)	90.317 (4)	90.135 (32)	89.93 (7)	90.018 (4)	89.863 (4)	89.863 (11)	89.554 (6)
Fe (z)	0.4930 (7)	0.4959 (5)	0.4942 (6)	[c]	[c]				
Te (z)	0.2172 (11)	0.2170 (5)	0.2181 (5)	[c]	[c]	0.2163 (5)	0.2184 (5)	0.2236 (11)	0.2214 (8)
Fe2 (z)	0.7995 (39)	0.7902 (25)	0.8017 (22)	[c]	[c]	0.8117 (32)	0.8190 (27)	0.824 (6)	0.8409 (23)
S (z)	0.37 (27)[b]	0.33 (6)	0.32 (4)	[c]	[c]	0.314 (23)	0.306 (14)	0.311 (18)	0.317 (8)
Fe2 occupancy	0.121 (5)	0.119 (3)	0.123 (3)	[c]	[c]	0.102 (5)	0.100 (3)	0.069 (7)	
phase fraction (%)	100	100	89 (2)	11 (2)	6.8 (8)	93.2 (8)	100	100	100

[a] The orthorhombic atomic positions are Fe (0.75 0.25 *z*), Te (0.25 0.25 *z*), interstitial Fe2 (0.25 0.25 *z*), and S (0.25 0.25 z). The tetragonal phase possess atomic positions of Fe (0.75 0.25 0.5), Te (0.25 0.25 *z*), interstitial Fe2 (0.25 0.25 *z*), and S (0.25 0.25 *z*). [b] The crystallographic information for the sulfur position in $Fe_{1+x}Te_{0.9925}S_{0.0075}$ has large error bars due to the very low occupancy. [c] The atomic positions of the minor phase in $Fe_{1+x}Te_{0.975}S_{0.025}$ and $Fe_{1+x}Te_{0.95}S_{0.05}$ were fixed to the values obtained in the majority phase of the neighboring composition, due to instability resulting from such low phase fraction. Errors represent one standard deviation.

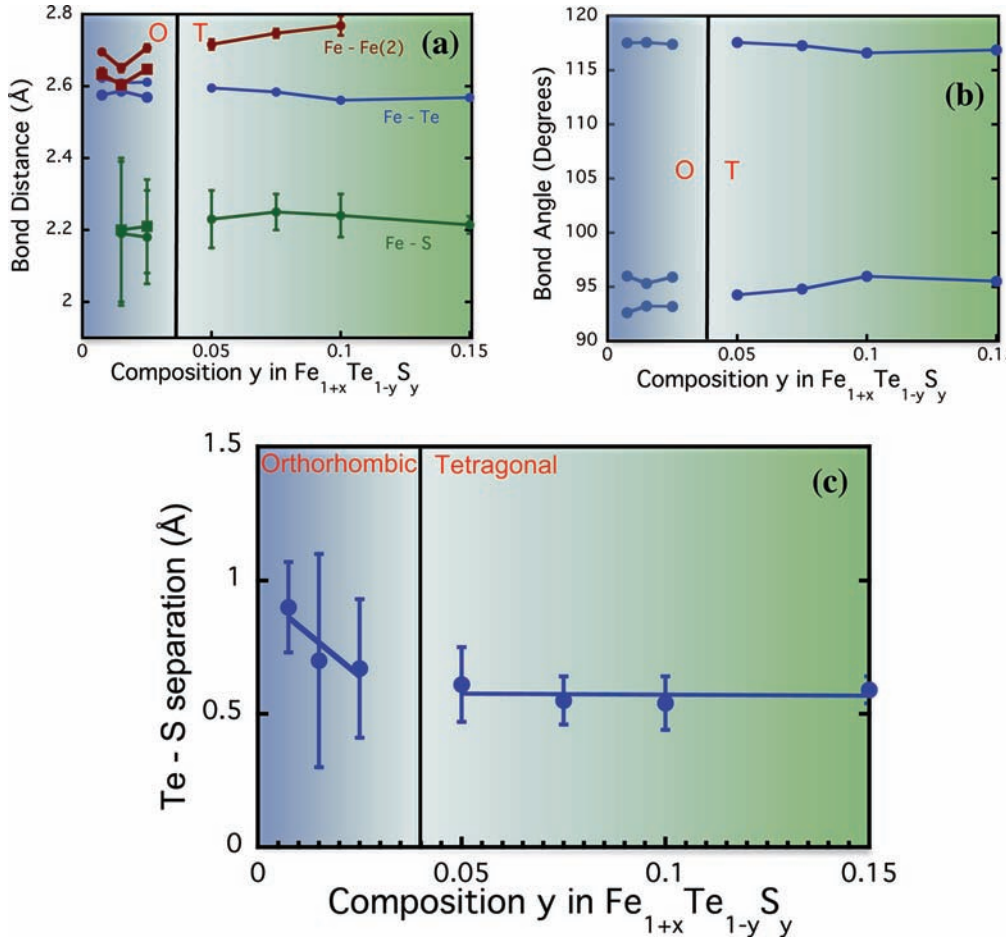

Figure 5. (a) Iron bond distances, (b) Fe−(Te, S) bond angles and (c) separation in the S and Te anion positions in the $Fe_{1+x}Te_{1-y}S_y$ series, obtained from fitting the powder neutron diffraction pattern at 4 K. All error bars, which represent one standard deviation, are included, however some are smaller than the symbols.

The Shannon and Prewitt ionic radii for six-coordinated Te^{2-}, Se^{2-}, and S^{2-} are 2.21, 1.98, and 1.84 Å, respectively.[36] The extensive difference between these anions can explain the inhomogeneity within the crystals and the tendency to form Te and S rich regions, which ultimately leads to the phase separation at low temperature in $Fe_{1+x}Te_{1-y}S_y$, when *y* is near the tetragonal−orthorhombic composition boundary and some of the sample undergoes a structural phase transition while another part remains tetragonal. The extent of the phase separation is expected to be greater and more detectable in the sulfur-doped systems than the analogous Se compounds due to greater size difference.

(36) Shannon, R. D. *Acta Crystalogr. A* **1976**, *32*, 751.

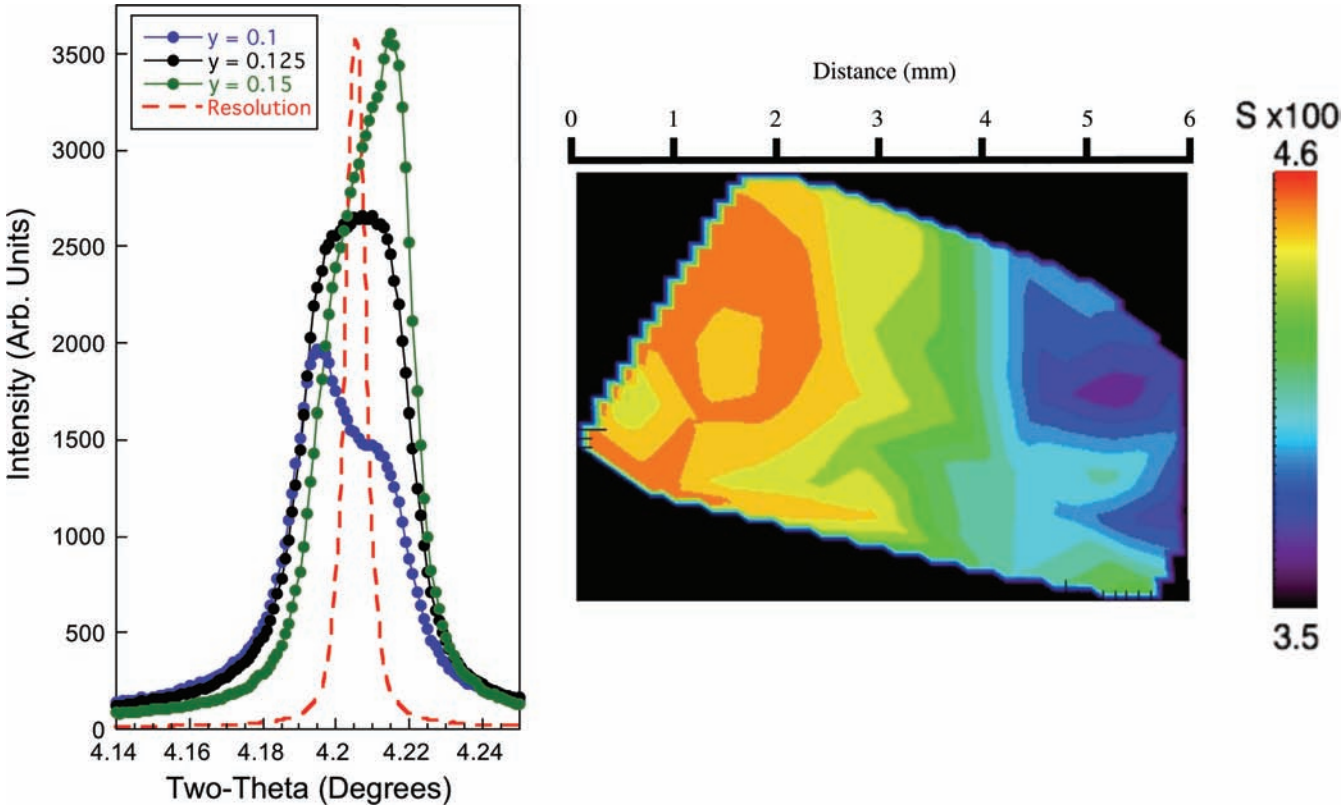

Figure 6. (a) Comparison of the (001) peak width as obtained from synchrotron powder X-ray diffraction, in $Fe_{1+x}Te_{1-y}S_y$ with a LaB6 660a standard, demonstrating significant sample broadening. (b) Composition variation of a single crystal with nominal formula, $Fe_{1+x}Te_{0.95}S_{0.05}$ as determined by *xy* mapping using wavelength dispersive spectroscopy. A total of 39 positions spread evenly over the crystal were measured to generate the map using the DAVE software.[47]

Optimal superconductivity in $Fe_{1+x}Te_{1-y}Se_y$ occurs at $x \approx 0.5$,[33] which gives an average anion size of ~2.095 Å, which is very similar to the average anion radius (2.1545 Å) achieved with the 15% doping of the much smaller S ion in $Fe_{1.0}Te_{0.85}S_{0.15}$, implying that structural considerations are important in understanding the optimal superconducting samples. Another property of the chalcogenide anion to consider is that of its electronegativity. While Pauling electronegativities of S and Se are quite similar (2.58 and 2.55, respectively), the Te value of 2.1 is much lower and closer to the value for Fe(II) of 1.83.[37] An obvious consequence is that the interaction between Fe and Te is expected to be more covalent than that between Fe and Se/S. Nevertheless, since the electronegativites in S and Se are similar, differences in the optimal superconducting doping levels can be attributed to differences in the anion size alone. Since Hu et al did not take diffraction data on $Fe_{1+x}Te_{1-y}S_y$ below 80 K, they did not report the magnetic and structural phase separation. However, their resistivity measurements do show a coexistence of magnetic ordering and superconductivity for $y = 0.03$,[26] consistent with our phase diagram.

For both $Fe_{1+x}Te$ and $Fe_{1+x}Te_{1-y}S_y$ systems, the incommensurate magnetic structure possess orthorhombic nuclear symmetry and the nonmagnetic compositions possess tetragonal symmetry, further highlighting the direct correlation between the magnetism and lattice degrees of freedom across different groups of Fe-based superconductors. As the spin density wave and superconductivity compete with the same Fermi surface, it has been proposed that there should be little coexistence of the two states.[38] Therefore, the coexistence of phases to result from chemical inhomogeneity within the sample, rather than the intrinsic nature of the electronic structure, corroborates this prediction. Coexistence of superconductivity and magnetism, which occurs in some phase diagrams but not others, has been widely discussed, although the highest superconducting transition temperatures are always found in compositions with no long ranged magnetic order.[26,39−45] However, in the case of

(37) Pauling, L. *The Nature of the Chemical Bond*; Cornell University: Ithaca, NY, 1960.
(38) Singh, D. J.; Du, M.-H.; Zhang, L.; Subedi, A.; An, J. *Phys. C* **2009**, *469*, 886.
(39) Drew, A. J.; Pratt, F. L.; Lancaster, T.; Blundell, S. J.; Baker, P. J.; Liu, R. H.; Wu, G.; Chen, X. H.; Watanabe, I.; Malik, V. K.; Dubroka, A.; Kim, K. W.; Rossle, M.; Bernhard, C. *Phys. Rev. Lett.* **2008**, *101*, 097010.
(40) Bernhard, C.; Drew, A. J.; Schulz, L.; Malik, V. K.; Roessle, M.; Niedermayer, C.; Wolf, T.; Varma, G. D.; Mu, G.; Wen, H.-H.; Liu, H.; Wu, G.; Chen, X. H. *New J. Phys.* **2009**, *11*, 055050.
(41) Laplace, Y.; Bobroff, J.; Rullier-Albenque, F.; Colson, D.; Forget, A. *Phys. Rev. B* **2009**, *80*, 140501.
(42) Park, J.; Inosov, D.; Niedermayer, C.; Sun, G.; Haug, D.; Christensen, N.; Dinnebier, R.; Boris, A.; Drew, A.; Schulz, L.; Shapoval, T.; Wolff, U.; Neu, V.; Yang, X.; Lin, C.; Keimer, B.; Hinkov, V. *Phys. Rev. Lett.* **2009**, *102*, 117006.
(43) Khasanov, R.; Bendele, M.; Amato, A.; Babkevich, P.; Boothroyd, A.; Cervellino, A.; Conder, K.; Gvasaliya, S.; Keller, H.; Klauss, H.-H.; Luetkens, H.; Pomjakushin, V.; Pomjakushina, E.; Roessli, B. *Phys. Rev. B* **2009**, *80*, 140511.
(44) Ryan, D. H.; Cadogan, J. M.; Ritter, C.; Canepa, F.; Palenzona, A.; Putti, M. *Phys. Rev. B* **2009**, *80*, 220503.
(45) Zhang, Y.; Wei, J.; Ou, H.; Zhao, J.; Zhou, B.; Chen, F.; Xu, M.; He, C.; Wu, G.; Chen, H.; Arita, M.; Shimada, K.; Namatame, H.; Taniguchi, M.; Chen, X.; Feng, D. *Phys. Rev. Lett.* **2009**, *102*, 127003.

$Fe_{1+x}Te_{1-y}S_y$ this coexistence is unquestionably the result of an inhomogeneous distribution of anions.

Conclusion

In summary, $Fe_{1+x}Te_{1-y}S_y$ is an example of the Fe(Te, Se, S) family of superconductors that distinguish themselves from other iron based superconductors in numerous ways. We show that that on sulfur inclusion, the magnetism of monoclinic $Fe_{1+x}Te$ transforms through an orthorhombic phase with two-dimensional incommensurate short ranged magnetic scattering to a superconducting tetragonal phase, with optimal superconductivity occurring at $Fe_{1.0}Te_{0.85}S_{0.15}$. The composition variation within the sample was such that, for compositions around the orthorhombic−tetragonal boundary, phase separation occurs at low temperature. Furthermore, the superconducting transition temperature of 9 K for $FeTe_{0.85}S_{0.15}$ is consistent with the variation of transition temperature with bond variance (a measure of the extent of the tetrahedral distortion from the ideal 109.47° (see Figure S2), as previous noted.[22] In addition to their similar average anion radii, $Fe_{1+x}Te_{1-y}Se_y$ and $Fe_{1+x}Te_{1-y}S_y$ both show optimal superconductivity at compositions with little or no excess iron, the control of which will be essential in understanding the relative importance of these factors. Recent work has identified new chemical procedures to deintercalate the excess iron from the $Fe_{1+x}Te$ system, which will prove important in understanding and expanding the Fe−Te−Se−S phase diagram.[46]

Acknowledgment. Use of the Advanced Photon Source at Argonne National Laboratory was supported by the U.S. Department of Energy, Office of Science, Office of Basic Energy Sciences, under Contract No. DE-AC02-06CH11357.

Supporting Information Available: Lattice parameters from powder X-ray diffraction as a function of nominal starting compositions, resistivity of $Fe_{1+x}Te_{0.875}S_{0.125}$ and $Fe_{1+x}Te_{0.85}S_{0.15}$ and the bond variance for various families of superconductors. Structural parameter (.cif) file of $Fe_{1.123(5)}Te_{0.948(4)}S_{0.052(4)}$ from single crystal X-ray diffraction. This material is available free of charge via the Internet at http://pubs.acs.org.

JA105279P

(46) Rodriguez, E. E.; Zavalij, P.; Hsieh, P.-Y.; Green, M. A. *J. Am. Chem. Soc.* **2010**, *132*, 10006.
(47) Azuah, R. T.; Kneller, L. R.; Qui, Y.; Tregenna-Piggott, P. L. W.; Brown, C. M.; Copley, J. R. D.; Dimeo, R. M. *J. Res. Natl. Inst. Stand. Technol.* **2009**, *114*, 341.